 ICES-2022-182

Development of a miniature heat exchanger for mechanically pumped loop systems for active thermal control of CubeSats

T.V. Ganzeboom[1], J. van Es[2]
Netherlands Aerospace Centre, Marknesse, The Netherlands

L. Formisani[3]
Delft University of Technology, Delft, The Netherlands

The relatively high power density of CubeSats results in large amounts of heat generated that needs to be dissipated to prevent overheating of a satellite's components. At present, passive thermal control means are used to resolve CubeSats thermal issues, however, as these satellites evolve, advanced active Thermal Control Systems (TCS) will be required. Especially the novel CubeSat propulsion systems require dedicated TCS for the propulsion unit and the corresponding electronics.

A promising type of TCS for CubeSats was determined to be the Mini-Mechanically Pumped fluid Loop (Mini-MPL). One such system has been developed at the Royal Netherlands Aerospace Centre (NLR), which consists of a single phase fluid loop that is used for component cooling. One of the important components of this system is the interface (I/F) with the Payload.

Three custom designed Miniature Payload Heat Exchangers (MPHX) are presented in this paper. During the design phase, a tool which is able to evaluate the cooling performance of different MPHX models has been built. Using this tool, the three best designs in terms of cooling performance have been identified: the offset strip fin heat exchanger, and two straight channels configurations with respectively triangular and trapezoidal cross sections.

The heat exchangers are produced through additive manufacturing (using the Direct Metal Laser Melting method) which allows for greater flexibility and customization of the designs. The models are tested in a pumped fluid loop at the NLR's Thermal Management Facilities to confirm the results predicted in the design phase as well as feasibility of the DMLM fabrication method.

Nomenclature

c_p	=	Specific heat capacity (W/kg K)
h	=	Heat transfer coefficient (W/m^2K)
k	=	Thermal conductivity (W/m K)
$\dot{m}$	=	Mass flow (kg/s)
M	=	Mass (kg)
P	=	Power (W)
R	=	Thermal resistance (K/W)
T	=	Temperature (K)
COTS	=	Commercial-off-the-shelf
DMLM	=	Direct Metal Laser Melting
HX	=	Heat Exchanger
I/F	=	Interface
MPHX	=	Mini Payload Heat Exchanger
MPL	=	Mechanically Pumped fluid Loop
NLR	=	Royal Netherlands Aerospace Centre
P/L	=	Payload
TCS	=	Thermal Control System

[1] *Aerospace Systems Engineer, Energy Management Group Aerospace Division, Thomas.ganzeboom@nlr.nl*
[2] *Principal R&D Manager, Energy Management Group Aerospace Division, Johannes.van.es@nlr.nl*
[3] *Master student Aerospace Engineering, Delft University of Technology, Ludovica.formisani@gmail.com*

I. Introduction

Miniaturization is one of the biggest trends of the space industry nowadays. In particular, CubeSats are being preferred over regular satellites thanks to their dimensions which brings a reduction in launch cost and development investment. Because of the reduced investment at stake, CubeSat developers are able to take larger risks when sourcing components for their satellite. One such example is the use of commercial-off-the-shelf (COTS) electronics in CubeSats which allows designers to make very capable systems at an affordable price. However, it has been shown that due to the use of miniaturized COTS electronics and the high power demand of on-board activities, the power density required by these systems is typically large when compared to traditional satellites [1]. This means that, in case of CubeSats, more power is being transformed into heat in the same volume, which can lead to thermal problems [2].

At present only passive thermal control systems are used for CubeSats, however as the power requirements increase, passive systems may not be suitable anymore for these applications. In order to overcome this issue, an active Thermal Control System has been designed at the Royal Netherlands Aerospace Centre. This system, which is called the Mechanically Pumped fluid Loop (or mini MPL), is a single phase fluid loop that is able to transport heat by pumping the fluid in the loop, see Figure 1. Among the critical components of this system, the mini payload heat exchanger is of interest for this project. Although commercially available heat exchangers exist, these are typically too large, too heavy or impractical for use in the space environment. Moreover, the integration of the mini MPL in CubeSat platforms introduces additional compatibility challenges linked to the limited available volume.

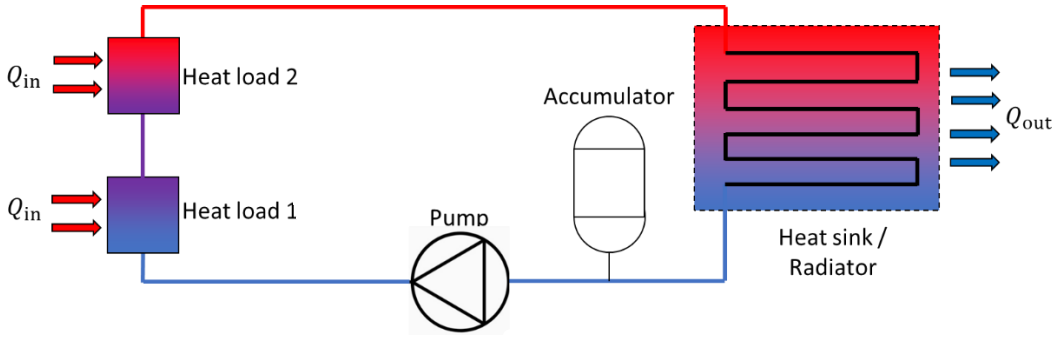

Figure 1. Schematic of a mechanically pumped fluid loop.

II. Requirements for a miniature heat exchanger for CubeSats

Requirements for a miniature heat exchanger for use in mechanically pumped loops in CubeSats have been defined.

- *Total heat transferred*
  It is expected that near-future CubeSats that require a mechanically pumped fluid loop as thermal control system would only require from 10 W to at most 100 W of heat [2]. Hence the heat exchanger design will be optimized for heat transfer in that range.

- *Single phase heat transfer*
  The heat exchanger design is based on a single phase heat transfer concept. For miniature channels single phase heat transfer, flows are assumed to be laminar.

- *Size and scalability*
  Due to the limited available volume on board CubeSats the miniature heat exchanger must indeed be miniature. The target utilized area is 20 mm x 20mm with a maximum height of 10 mm. In some cases, the aforementioned size requirement can be different than stated here, the heat exchanger must therefore be able to scale up to at least doubled dimensions (40 mm x 40mm) and down to at least half the dimension (10 mm x 10 mm) with the same height restriction.

- *Pressure drop*
  A mechanically pumped fluid loop on board of a CubeSat is limited in its pumping capacity, therefore the pressure drop of the heat exchanger module must be minimized. A lower pressure drop would also allow for multiple heat exchangers to be connected in series.

- *Low mass & cost*
  Mass and costs are a critical aspect for the heat exchanger design. The choice of material and design must be focussed on minimizing mass while optimizing performance and production cost.

- *Reliability & manufacturing*
  Another important requirement is the manufacturing technique and reliability. The manufacturing technique must allow for flexibility in design, scalability as well as reliability with respect to effective operation and leak-tightness.

For the internal geometry several different design concepts have been investigated. These can be broken down into two categories; parallel channels and 'other' concepts.

1. Parallel channels

This category is the traditional heat exchanger design where multiple channels with the same geometry are placed in parallel to effectuate cooling. In the design phase the following channel geometries are considered: circular, trapezoidal and triangular. These geometries are shown in Figure 2.

Circular *Trapezoidal* *Triangular*

Figure 2. Channel geometries for parallel channels under consideration

2. 'Other' concepts

In the second category are placed the heat exchanger designs that do not have parallel channels. The designs considered in this project are no-channels e.g. an open space and the offset strip fin geometry. The open space design is a rectangular single channel design spanning the entire width of the heat exchanger and is used as a reference model. An example of the offset strip fin geometry is shown in Figure 3.

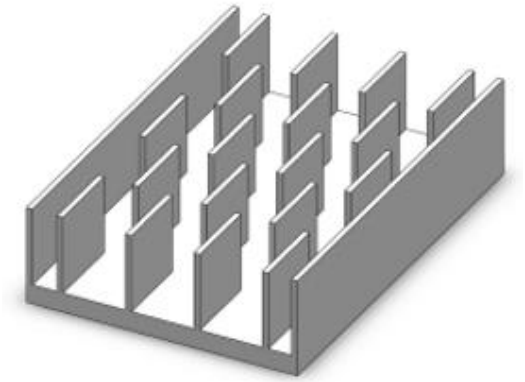

Figure 3. Offset strip-fin design concept [3].

III. Heat exchanger modelling

A thermal and fluidic model for simulating different heat exchanger concepts has been designed. For the thermal model the situation as shown in Figure 4 has been used as a starting point.

A. Thermal model

The component of interest for this study is the payload (P/L) side of the cooling loop, this is modelled by breaking this side up in a heating component mounted on a support structure and heat exchanger with coolant, as shown in Figure 4. Heat is generated at the heat source which is transferred to the heat exchanger block through contact conductance. The white layer represents thermal interface material to improve contact conductance. The liquid

coolant flows through the heat exchanger where it takes up heat. Heat transfer through the support structure or mounting assembly is not modelled.

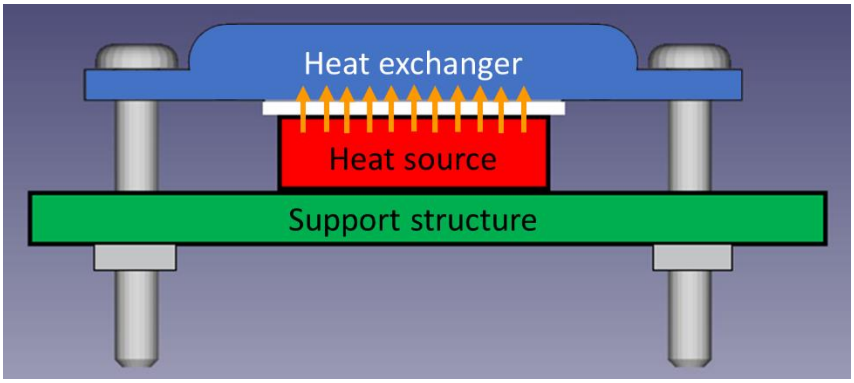

Figure 4. Thermal model setup.

The heat transfer has been modelled by separately analysing each component and by considering a balance of the in and out heat flows. The P/L is modelled as a single node heat source and generates heat (P) in Watts. The heat transfer between the payload and heat exchanger blocks is modelled using Equation (1).

$$\frac{dT_p}{dt} = \frac{P - Q_{ph}}{M_p c_{p,p}} \tag{1}$$

Here M_p is the mass and $c_{p,p}$ is the specific heat capacity of the P/L. T_p is the temperature in the payload. The heat transferred to the heat exchanger block, Q_{ph}, is based on the contact conductance of the payload with the heat exchanger. Using a thermal interface material with a thermal conductivity k_{int}, thickness t_{int}, and a total contact area A_{cond}, the heat transferred can be calculated:

$$Q_{ph} = \frac{k_{int}}{t_{int}} A_{cond}(T_p - T_h) \tag{2}$$

Where T_h is the contact temperature of the heat exchanger block.

The same procedure is followed to model the heat exchanger block, with the exception that in this case heat is received from the payload through conduction and transferred to the fluid through convection.

$$\frac{dT_h}{dt} = \frac{Q_{ph} - Q_{hf}}{M_h c_{p,h}} \tag{3}$$

$$Q_{hf} = hA_{conv}(T_h - T_f) \tag{4}$$

Here *h* is the convective heat transfer coefficient, A_{conv} is the contact area between heat exchanger and fluid, and T_f is the fluid's temperature.

Finally, the heat transferred by convection is used to heat up the fluid, which final temperature can be calculated with the heat transfer equation:

$$T_{f,out} = T_{f,in} + \frac{Q_{hf}}{\dot{m} c_{p,f}} \tag{5}$$

Where $\dot{m}$ is the fluid mass flow with specific heat capacity $c_{p,f}$, and Q_{hf} is the heat transferred from the heat exchanger to the fluid.
By solving these equations numerically, it is possible to obtain the temperature profiles of payload, heat exchanger and fluid during the heat transfer process.

B. Fluidic model

The fluidic model aims to determine two important characteristics of the heat exchanger in combination with a certain flow. These are the convective heat transfer coefficient between the heat exchanger and the fluid and pressure drop of the fluid across the heat exchanger.

1. Convective heat transfer coefficient

The convective heat transfer coefficient is calculated using Equation (6).

$$h = \mathrm{Nu}\frac{k}{D_h} \tag{6}$$

Where k is the thermal conductivity of the fluid and D_h the hydraulic diameter of the channel geometry under investigation. The Nusselt number and hydraulic diameter are determined per geometry based on correlations from literature. The resulting heat transfer coefficient is then used in Equation (*4*) of the thermal model.

For straight channels the model from Ref. [4] is applied, which can be used for a broad range of channel geometries. This model is based on several assumptions. The first assumption is that the model is dealing with a constant axial wall heat flux with constant peripheral wall temperature (also called "H1" boundary condition). This assumption can be justified by the fact that the length and width of the heat exchanger is small and the material thermal conductivity high. Further, the model assumes fully developed, steady state, laminar and continuum flow, incompressible flow, constant viscosity and thermal conductivity, negligible viscous dissipation and surface effects, and constant cross sectional area and perimeter. The assumptions on flow state are justified by the fact that for a miniature heat exchanger the channel diameter is small and the flow is single phase. The constant viscosity and thermal conductivity assumptions do introduce an error as well as the lack of surface effects.

For the offset strip fin geometry the model described in Ref. [5] is used. This model gives the flexibility to change the length, width and separation distance for the fins that are placed in the flow. However, it must be noted that the authors of Ref. [5] indicate that this model has an accuracy of 20% since this design is difficult to model.

2. Fluidic pressure drop

For the fluidic pressure drop in the heat exchanger only the frictional pressure drop is considered. This is calculated using the Darcy-Weisbach equation.

$$\Delta \mathrm{p} = \frac{1}{2}\frac{f\rho u_m^2 L}{D_h} \tag{7}$$

Where ρ is the fluid density, u_m is the mean flow velocity in the channel and f is the Darcy friction factor, and it depends on flow and surface conditions, and channel wall geometry. The friction factor is then calculated for laminar flows [6].

$$f = 4\frac{Po}{Re} \tag{8}$$

Where Po is the Poiseuille number ($Po = fRe$) and the factor 4 has been added for conversion from Fanning to Darcy formula. It can be shown that for a circular tube $Po = 16$, while for rectangular channels it can vary based on the aspect ratio: from 14.23 (square channel) to 24 (aspect ratio tends to infinity). Other values for typical channel cross sections are given in Ref. [7].

For the offset strip fin designs the model from Ref. [8] is applied using the following equation.

$$\Delta \mathrm{p} = \frac{\rho_\mathrm{f} \mathrm{u}_\mathrm{m}^2}{2}\left[(\mathrm{K_c} + 1 - \sigma^2) + \mathrm{f}\left(\frac{4\mathrm{L}}{\mathrm{D_h}}\right) - (1 - \sigma^2 - \mathrm{K_e})\right] \tag{9}$$

Where σ is a parameter related to the heat sink's geometry ($\sigma = \frac{\mathrm{s-b}}{\mathrm{s}}$) with *s* and *b* the lateral spacing and width of the fins respectively. Using σ, $\mathrm{K_c}$ and $\mathrm{K_e}$ can be calculated which are respectively the coefficient of abrupt contraction and expansion:

$$K_c = -0.4446\sigma^2 + 0.0487\sigma + 0.7967$$
$$K_e = 0.9732\sigma^2 - 2.3668\sigma + 0.9973 \quad (10)$$

Also in this case f is the Darcy friction factor, and its correlation has been given by:

$$f = 9.6243Re^{-0.7422}\alpha^{-0.1856}\delta^{0.3053}\gamma^{-0.2659} \times \left[1 + 7.669 \times 10^{-8}Re^{4.429}\alpha^{0.920}\delta^{3.767}\gamma^{0.236}\right]^{0.1} \quad (11)$$

Where the parameters α, γ and δ are parameters of the fins in the flow.

IV. Heat exchanger design & production

The preliminary design phase has been dedicated to the identification heat exchanger designs that satisfy the requirements. In the detailed design phase, the three best designs will be selected to perform a deeper study. This was done by modelling the mini mechanically pumped fluid loop as described in Ref. [2] using the same parameters such as working fluid and expected mass flow. Other limitations are in the length of the channels (20 mm) and the number of channels in parallel. This last parameter is calculated based on the width of the heat exchanger (20 mm) divided by the diameter of a single channel plus a total wall thickness of 5 mm. For the five heat exchanger geometries mentioned earlier, this has been modelled and the results are shown in Figure 6. Here the specific heat transfer coefficient is plotted against the non-dimensional Bejan number representing single phase pressure drop across the heat exchanger. The Bejan number in the context of mass transfer is defined as

$$Be_L = \frac{\Delta p\, L^2}{\mu D_h} \quad (5)$$

Where Δp is the calculated pressure drop, L is the length of each channel, μ is the dynamic viscosity of the working fluid and D_h is the hydraulic diameter. The specific heat transfer coefficient is expressed in Watts per Kelvin, and it is calculated by multiplying the heat transfer coefficient of the heat exchanger by the contact area between fluid and heat exchanger. This parameter was considered more suitable for the analysis than the standard heat transfer coefficient (W/m^2K) because it allows to compare heat exchanger models with different internal geometries.

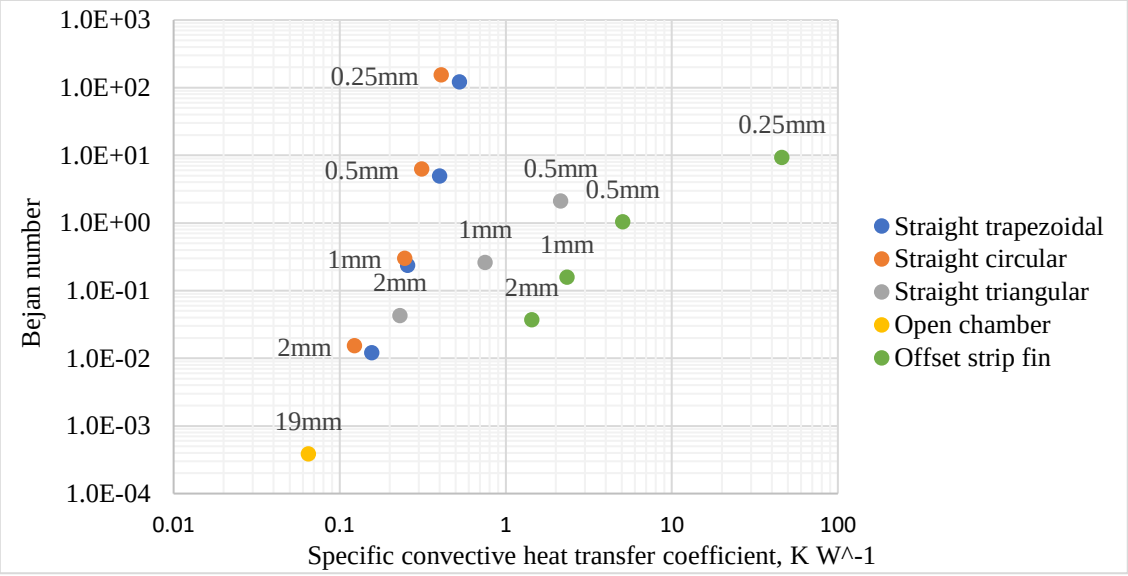

Figure 6: Heat exchanger performance of several heat exchanger designs with an area of 20 mm x 20 mm and a heat exchanger height of 5 mm. The dimension mentioned is the width of the channel for the straight and open channels. For the offset strip fin the dimension is the distance between two fins in the same row.

It is possible to notice that the offset strip fin returns the best performance both in terms of pressure drop and specific convective heat transfer coefficient. Additionally, the triangular channels and the trapezoidal channels give promising results. The preliminary design phase allowed to identify these three design options in terms of

pressure drop and thermal performance: straight channels heat exchangers with triangular (Double Triangle HX) and trapezoidal (Double Trapezoid HX) cross sections, and offset strip fins. All these options have been modelled in the CAD environment for a contact area with the payload of 20 x 20 mm and a target mass of maximum 10 grams and are hereby described in more detail.

A. Straight channels double triangle heat exchanger

This component is formed by 24 straight channels with triangular cross sections. In order to maximize the contact area between fluid and HX, the triangular channels are in an "interlocked" position (from here the attribute "double"), with the bases of adjacent triangles placed in opposite sides of the HX (top or bottom), as shown in Figure 7.

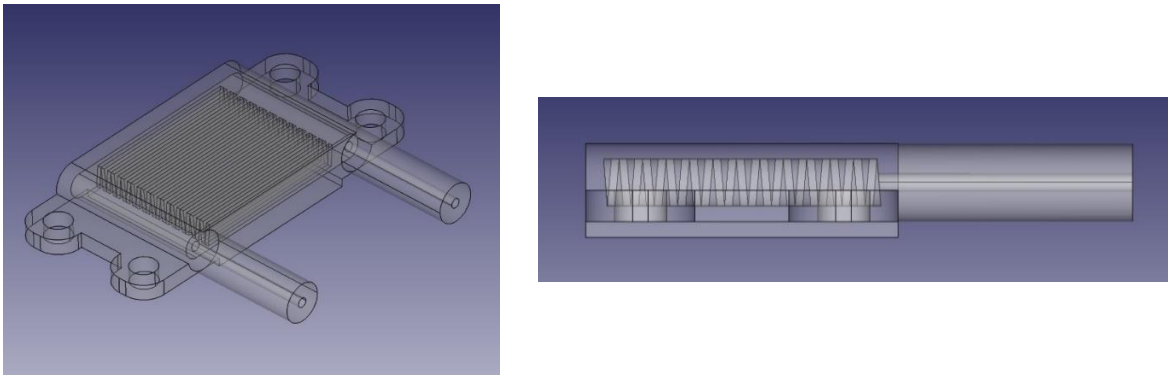

(a) **(b)**

Figure 7. Double Triangle HX CAD model.

In particular, each channel's cross section is an isosceles triangle with a base of 0.5 mm, 3 mm high, and channel spacing is 0.5 mm. The heat exchanger's total dimensions (without the mounting plate) are 20 x 20 x 5 mm, with inlet tubes of 15 mm. It has to be noted that the CAD drawings include parts that will need to be machined after the printing. In particular, these are the area of contact between payload and HX, which as heat transferring surface will need to be as smooth as possible, and the inlet and outlet tubes, which diameter will be reduced to 1/8" for compatibility with the hydraulic fittings. Finally, a mounting plate has been added to ensure good contact between the interfaces, and it is suited for M3 bolts.

B. Straight channels double trapezoid heat exchanger

This model has the same "interlocked" channels' structure as the triangular heat exchanger, with the exception that in this case the cross sections have a trapezoidal shape. The total number of channels is now down to 17. The internal structure of the trapezoid heat exchanger is shown in Figure 8.

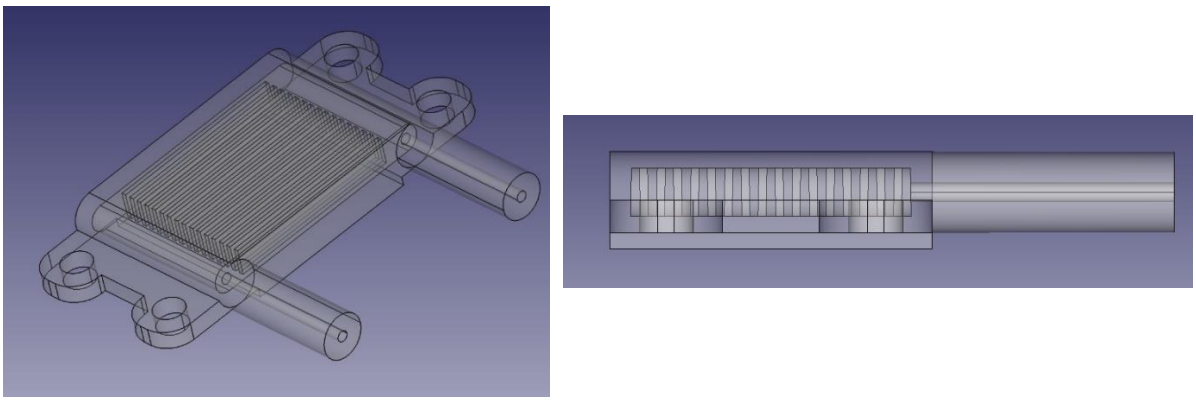

(a) **(b)**

Figure 8. Double Trapezoid HX CAD model.

In particular, each channel's cross section is an isosceles trapezoid with bases of 0.5 mm and 0.6 mm, an height of 3 mm and a channel spacing of 0.5 mm. Again, the heat exchanger is 20 x 20 mm, and 5 mm high. The values

of the bases suggest that the cross sections are almost rectangles, however the slightly trapezoidal shape has been chosen for pressure drop reasons and to have a slightly bigger contact area for heat transfer. All the notes about surface refinement and mounting plates that have been done for the triangular heat exchanger are also valid for this case.

C. Offset strip fin heat exchanger

The offset strip fins heat exchanger (Figure 9) is formed by respectively 12 and 11 fins alternated in the fluid direction to form a checkered pattern as shown in Figure 9b.

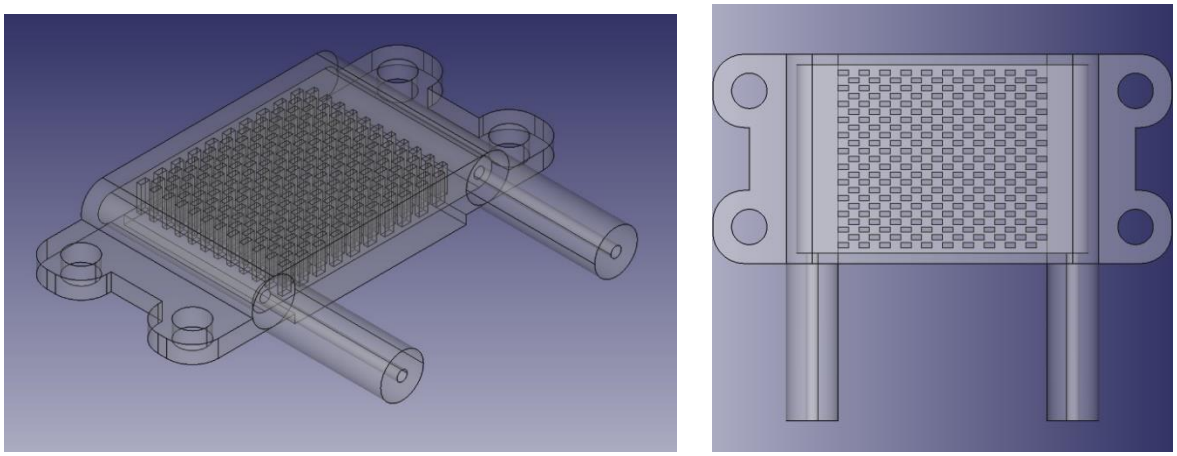

(a) **(b)**

Figure 9. Offset strip fins HX CAD model.

Each fin is 0.5 x 1 mm and 3 mm high, with a fin spacing of 1 mm. Again, the heat exchanger's dimensions are 20 x 20 mm and a total height of 5 mm. All the notes about surface refinement and mounting plate are valid.

D. Metal 3d printing

The NLR's Additive Manufacturing department has been responsible for the production of the to-be-tested heat exchanger models. It should be noted that two copies of each component have been made to increase the reliability of the test results. The printing setup and orientation of the heat exchangers is shown in Figure 10. The material used for the printing is the Aluminum alloy AlSi10Mg.

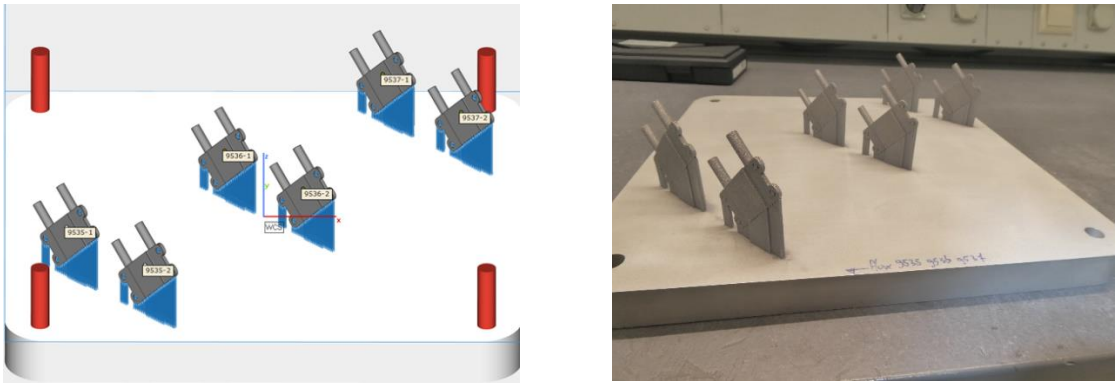

(a) Schematic of printing setup. (b) Parts after printing.

Figure 10. heat exchangers printing setup.

The parts have been printed using the Powder Bed Fusion technique, which consists in distributing a fine layer of powder over a build plate and selectively melt a cross section of the part into the powder layer. To do so, a Selective Laser Melting (SLM) machine has been used, which fuses metal layers into parts thanks to high powered lasers.

Several constraints have been taken into account when determining print orientation:

- To guarantee leak tight walls, outer walls should be at least 1 mm thick.
- A build direction such that the cross sectional area is minimal should be determined.
- Overhang (angles lower than 45 degrees) is avoided along the build direction.
- Small channels have the best quality if printed in vertical direction.
- A machining offset on the outside diameter of the tubes should be added depending on the method used to connect the HXs to the loop. This is because printed tubes tend to be quite rough and thus need to be machined to ensure a right fit of the hydraulic connectors. Moreover, also all the heat transferring surfaces should be designed with a machining offset of about 1 mm to allow for surface refinement.

In particular, to meet the last constraint, the heat exchangers were subsequently brought to the workshop for surface refinement. The finished parts are shown in Figure 11.

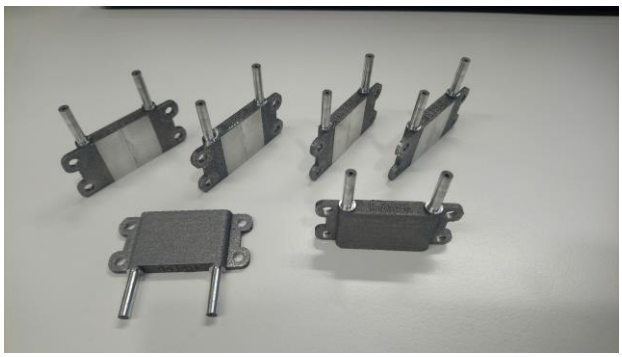

Figure 11. Printed parts after surface refinement.

Each heat exchanger has been weighed after surface refinement, and results are shown in Table 1.

Table 1. Mass of heat exchanger with and without hydraulic fittings.

	w/o hydraulic connections	w/ hydraulic connections
Triangle	7.68 g	21.50 g
Trapezoid	7.22 g	21.14 g
Offset	6.70 g	20.43 g

The heat exchangers have been designed with a target mass of 10 grams, which is indeed achieved by looking at the second column of Table 1. However, it is also possible to notice that the hydraulic fittings almost triple the total mass. This is indeed a disadvantage of the chosen connections and future work should be focused to find a way of connecting the heat exchanger with the rest of the loop without considerably increasing the component's total mass.

V. Heat exchanger testing

Each of the six printed components has been subjected to two tests: a differential pressure measurement and a payload power test. The differential pressure measurement is done to assess whether the tool predicts accurately the pressure drop in the microchannels. The pressure values have been recorded for different mass flows so to be able to obtain a mass flow-pressure drop relation by interpolation of the test results. After the pressure drop measurements, each component has been tested for a payload power of 5, 10, 15, 20 and 30 Watts.

A. Pressure drop testing

The results of the pressure drop measurements for all the design models are shown in Table 2. A breakdown of the expected contributions of each component to the total pressure drop value has also been added.

Table 2. Total expected and measured pressure drop of the heat exchangers.

HX type	Source	Pressure drop [mbar]	Difference from model
Double triangle	*Microchannels*	*2.03*	
	Manifolds	*1.62*	
	I/O fittings	*23.30*	
	Connecting tube	*106.31*	
	Total dP (expected)	**133.25**	
	Total dP measured	**143.43**	8%
Double trapezoid	*Microchannels*	*0.32*	
	Manifolds	*1.01*	
	I/O fittings	*23.30*	
	Connecting tube	*106.31*	
	Total dP (expected)	**130.93**	
	Total dP measured	**143.78**	10%
Offset strip fins	*Microchannels*	*0.42*	
	Manifolds	*0.84*	
	I/O fittings	*23.30*	
	Connecting tube	*106.31*	
	Total dP (expected)	**130.86**	
	Total dP measured	**145.34**	11%

It is possible to notice that the pressure drop in the heat exchanger has been predicted by the model with a worst accuracy of 11 % given by the offset strip fins case. While the pressure drop expected in the heat exchanger components is still in agreement with the requirements, attention should be paid to the contributions of the other components of the setup, such as the connecting tubes and the fittings.

On this regard, the pipe's roughness has been identified as the main responsible of the increased pressure drop in the heat exchanger. A sensitivity analysis on the pressure drop with respect of the inner diameter of circular tubes for different surface roughness values has been performed, and the results are shown in Figure 12.

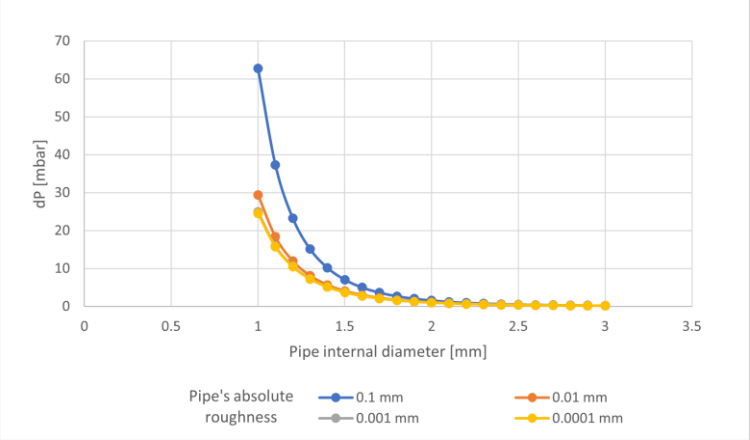

Figure 12. Pressure drops in HX's inlet and outlet circular pipes.

It is possible to notice that in the region of pipe internal diameters between 1 mm and 1.5 mm there is a strong dependence of the pressure drop with respect to both diameter and pipe roughness. A difference of almost 30 mbar for 1 mm internal diameters can be noticed between pipes with 0.1 mm and 0.01 mm roughness. This difference tends to decrease with increased roughness, until the curves start to overlap for values smaller than 0.001 mm.

B. Thermal performance testing

The developed model evaluates the thermal performance of the heat exchanger by solving a differential equations problem. This gives as output the temperature profiles of the payload, exiting fluid and heat exchanger from the start-up phase until a steady state is reached. In the testing scenario, the temperature profiles can be built using the temperature measurements performed by thermocouples. The setup used is shown in Figure 13.

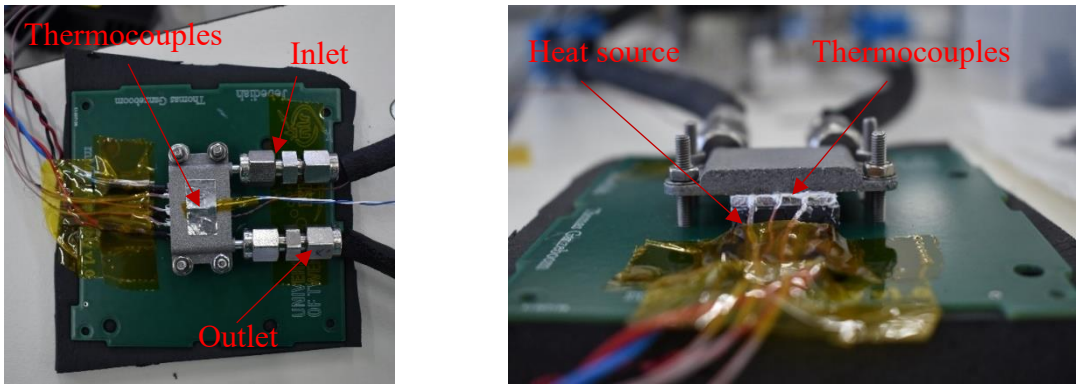

Figure 13. Heat exchanger integrated into thermal performance test setup. During testing the setup is thermally insulated. Top view (left) and side view (right).

Hereby all the results obtained for each heat exchanger type and for different payload power conditions will be presented and discussed. In particular, the results for the payload power cases of 20 and 30 Watts have been identified as most relevant for this study.
Figure 14 shows the results for the thermal performance testing of the Double Triangle HX. The solid line indicates the temperature profile predicted by the model, while the experimental data are represented as point values in the graphs.
It is possible to notice that, for both power cases, the temperature profiles are better predicted when considering a lower payload input power in the model. This happens because, as the payload power increases, the convection losses to the surrounding environment become more severe. These losses are due to the fact that the setup is not in vacuum, thus the surrounding air is the vector of convective heat transfer between the setup and the environment.
Convective losses can be quantified by computing the actual power that is absorbed by the fluid:

$$Q_{abs,fluid} = \dot{m} c_{p,f} (T_{out} - T_{in}) \quad (12)$$

Where $\dot{m}$ is the mass flow ($2g/s$), $c_{p,f}$ is the fluid's specific heat capacity (about $950\ J/kgK$), and T_{out} and T_{in} are respectively the outlet and inlet temperature of the fluid. Computing this value for the Double Triangle HX yields to an actual power absorbed by the fluid of respectively 17 Watts and 23 Watts. Using these power values as input to the model yields to a more accurate prediction of the temperature profiles, which goes from 11% with 20W input, to 1% using 17W, and from 16% with 30W input, to 2% using 23W.

The thermal performance for the Double Trapezoid HX is shown for both power cases in Figure 15. The same corrections made for the Double Triangle HX also apply in this case, reaching the same accuracies as the previous case.

The thermal performance of the offset strip fins heat exchanger is shown in Figure 16. Also in this case the model has been adapted to account for convection losses to the environment, getting however slightly lower accuracies than the previous cases: temperature profiles for 20W input power were predicted with 13% accuracy, which was lowered to 5% when using 17W. Analogously, for the 30W power case, the data from the experiments were predicted within a 26% margin from the simulation values, which was lowered to 16% using an input power of 24W.

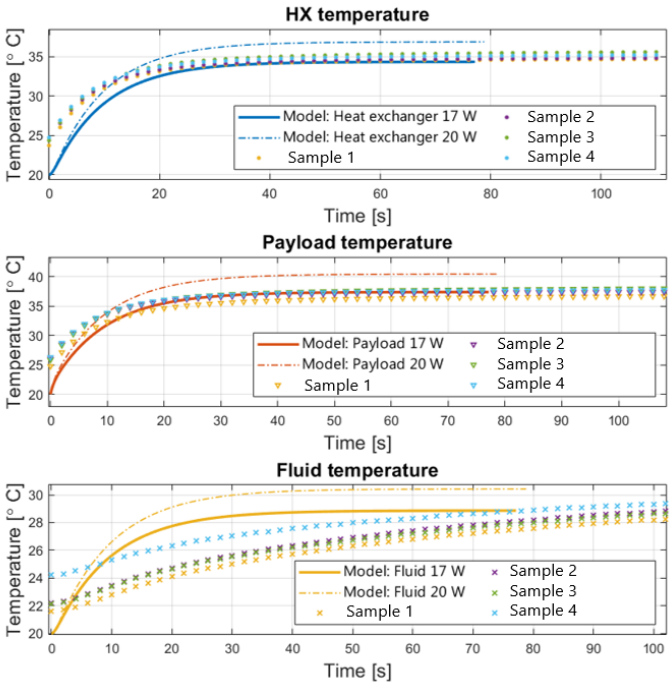

(a) Power case 20 Watts

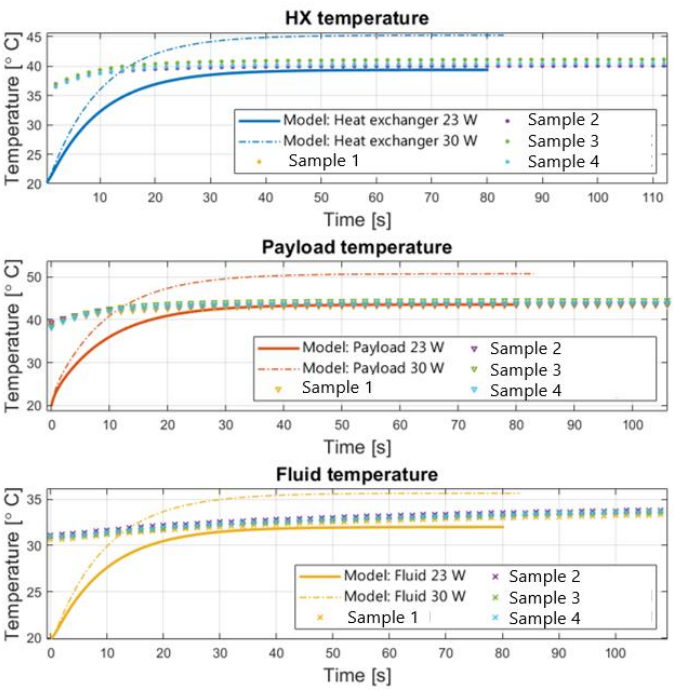

(b) Power case 30 Watts

Figure 14. Double Triangle HX thermal performance results.

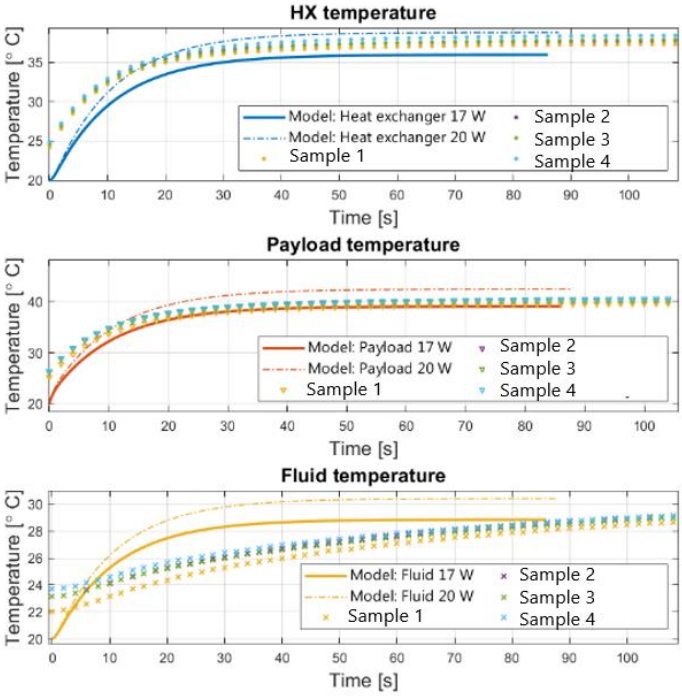

(a) Payload power 20 Watts

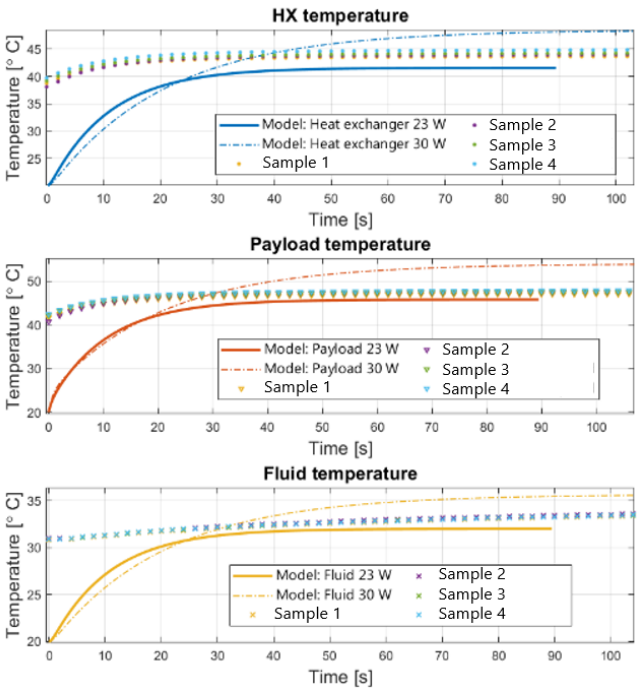

(b) Payload power 30 Watts

Figure 15. Double Trapezoid HX thermal performance results.

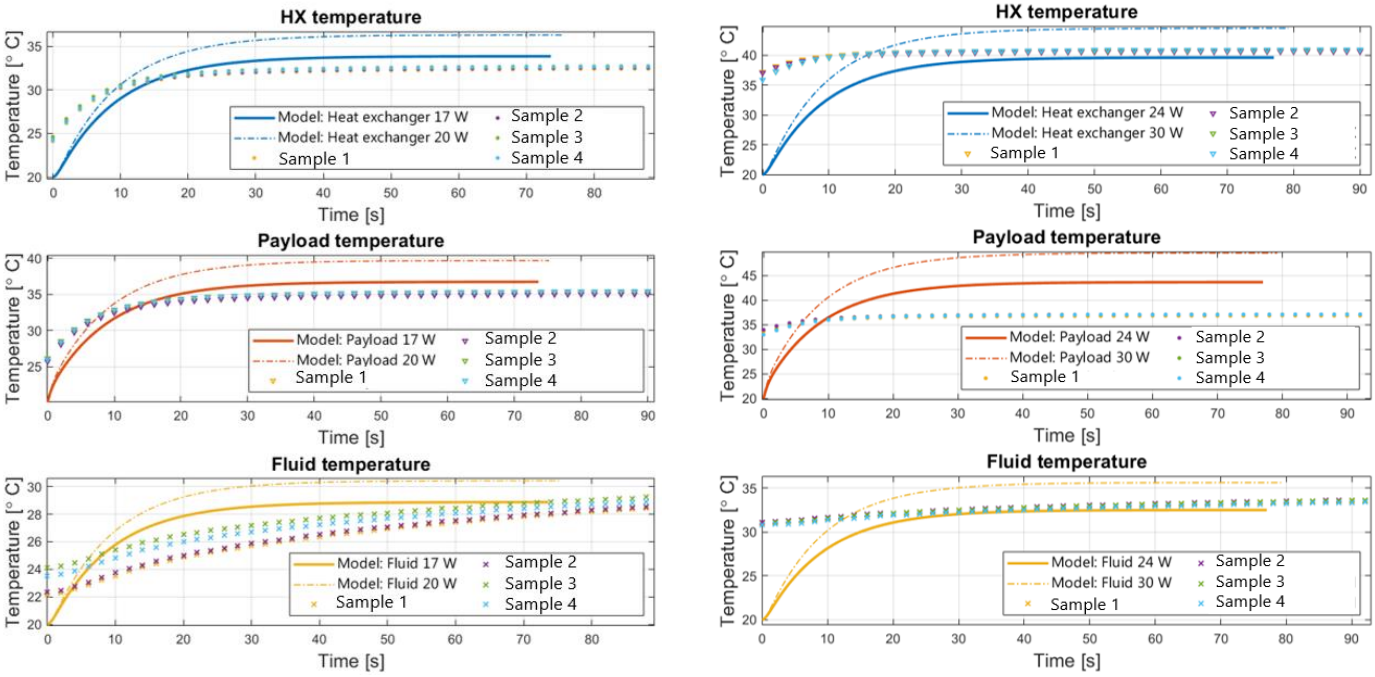

(a) Payload power 20 Watts.

(b) Payload power 30 Watts..

Figure 16. Offset strip fins thermal performance results.

C. Heat transfer coefficient

Table 3 shows a comparison between simulation and experiments of the heat transfer coefficient h and the convective thermal resistance R_{HX}. In case of the experimental data, these values have been calculated as follows:

$$h = \frac{P_{payload}}{A_{contact}(T_{HX} - T_{fluid})} \tag{13}$$

Where T_{HX} is the average between the temperatures measured on top of the HX and in the interface with the payload, and T_{fluid} is the average temperature between the inlet and outlet tubes. Each component has been tested for different power cases which yielded to slightly different values of the heat transfer coefficient, mostly linked to the testing conditions and the accuracy of the thermocouples. For this reason, the values in Table 3 are the result of an average between all the values obtained for the different power conditions.

Table 3. Heat transfer coefficient values for all heat exchangers

HX type	Component	h [W/m2K]	R [K/W] (20 mm x 20 mm area)	Difference from model
Double triangle	*Sample 1*	*776*	*0.440*	
	Sample 2	*826*	*0.413*	
	Sample average	**801**	**0.427**	
	Simulated	**731**	**0.467**	9%
Double trapezoid	*Sample 1*	*802*	*0.550*	
	Sample 2	*775*	*0.570*	
	Sample average	**788**	**0.560**	
	Simulated	**774**	**0.571**	2%
Offset strip fins	*Sample 1*	*1205*	*0.296*	
	Sample 2	*1182*	*0.302*	
	Sample average	**1194**	**0.299**	
	Simulated	**895**	**0.399**	11%

It is possible to notice that the model is slightly underestimating the values of both the heat transfer coefficient and the thermal resistance, with the worst accuracy of about 11 % in case of the offset strip fin heat exchanger. At the same time, the pressure drop is also under-estimated by the model.

Since the heat exchangers, manifolds and inlet and outlet tubes have been manufactured as a single component, it was not possible to accurately measure the surface roughness of the internal channels, which led lower accuracies in the model. In fact, the relatively high roughness affects the value of the Nusselt number in the channels by increasing the surface available for heat exchange, which in its turn increases the thermal performance of the heat exchanger at the expense of a higher pressure drop in the channels. This would explain the differences observed between the tests and the model.

VI. Conclusions

A Matlab based tool has been developed, and it was successfully able to predict the thermal performance and pressure drop for a specific heat exchanger with dimensions and materials set by the user. This tool has then been used to perform a detailed design study in order to identify the best heat exchanger configurations in terms of thermal performance, that will be then brought to the testing phase. As outcome of this analysis, three designs were identified: straight channel heat exchanger with triangular and trapezoidal cross sections, and the offset strip fin. These models have then been designed using CAD, and manufactured at the NLR additive manufacturing facilities.

Finally, all the produced heat exchangers have been tested using a mechanically pumped fluid loop, which has been built according to the structure of the mini MPL. In particular, two tests were performed: a differential pressure measurement, and a payload power test.

The thermal performance test show results within 11% accuracy with respect to the simulations. The model was able to predict the temperatures of the fluid as well as the heat exchanger component when compared with the laboratory tests. The pressure drop tests show overall results in agreement with the model. It was noted that in the current test setup the pressure drop in the heat exchanging part of the heat exchanger was not dominant, which makes it difficult to precisely determine if the pressure drop in that part of the component is in agreement with the model. Further research into this aspect as well as the influence of surface roughness is planned.

VII. References

[1] J. van Es, H. J. van Gerner and R. C. van Benthem, “Component Developments in Europe for Mechanically Pumped Loop Systems (MPLs) for Cooling Applications in Space,” in *46th International Conference on Environmental Systems*, Vienna, Austria, 2016.

[2] J. van Es, T. Ganzeboom, R. van den Berg, A. van Vliet, S. Elvik and H. Brouwer, “Mini mechanically pumped fluid loop design, modelling and tests for standardized CubeSat thermal control,” in *50th International Conference on Environmental Systems*, Lisbon, Portugal, 2021.

[3] Y. Ali, A. S. Bahman and F. Blaabjerg, “A modification of offset strip fin heatsink with high-performance cooling for lgbt modules,” in *Applied sciences 10*, 2020.

[4] E. Sadeghi, M. Bahrami and N. Djilali, “Estimation of Nusselt number in microchannels of arbitrary cross-section with constant axial heat flux,” in *International conference on nanochannels, microchannels, and minichannels*, 2008.

[5] M. M. Raj and A. E. Bergles, “Heat transfer and pressure drop correlation for the rectangular offset strip fin compact heat exchanger,” in *Experimental thermal and fluid science 10*, 1995.

[6] S. Kakaç, R. K. Shah and W. Aung, “Handbook of single-phase convective heat transfer,” 1987.

[7] S. Kandlikar, S. Garimella, D. Li, S. Colin and M. R. King, “Heat transfer and fluid flow in minichannels and microchannels,” 2005.

[8] S. Ndao, Y. Peles and M. K. Jensen, “Multi-objective thermal design optimization and comparative analysis of electronics cooling technologies,” in *International journal of heat and mass transfer 52*, 2009.